The Deformation of Clad Aluminum Sheet Produced By Direct Chill Casting

Article *in* Metallurgical and Materials Transactions A · August 2010

DOI: 10.1007/s11661-010-0298-z

3 authors, including:

Mark Gallerneault
Alcereco Inc.
57 PUBLICATIONS **506** CITATIONS
SEE PROFILE

Robert B. Wagstaff
Oculatus
16 PUBLICATIONS **155** CITATIONS
SEE PROFILE

The Deformation of Clad Aluminum Sheet Produced By Direct Chill Casting

DAVID J. LLOYD, MARK GALLERNEAULT, and ROBERT B. WAGSTAFF

The tensile and bending response of AA3003/AA6111 sheet produced by direct chill casting has been investigated. It is shown that the interface strength of the clad sheet has a minimum value of 175 MPa, and failure does not occur in the interface. The yield strength of the clad sheet obeys the rule of mixtures, and up to a cladding thickness of 100 μm—which was the thickest investigated—the work hardening behavior and tensile response are essentially unaffected by the presence of the cladding. The bending response of the sheet is improved greatly by the presence of ductile cladding, which was the case for prestrained and aged sheet. Under bending, failure is initiated in the lower bendability core and then eventually propagates through the more ductile cladding, which yields the final bend failure.

DOI: 10.1007/s11661-010-0298-z

I. INTRODUCTION

CLAD aluminum sheet is produced commercially by the roll bonding process; typical applications are brazing sheet in which a brazeable, usually an AlMn AA3000 series alloy, is clad with a low-melting-point AlSi AA4000 series alloy and an aerospace sheet in which a high-strength, but low-corrosion-resistant AlMgCu AA2000 or AlZnMgCu AA7000 series alloy is clad with a more corrosion-resistant dilute AA1000, AA2000, or AA7000 alloy. Roll bonding is a well-established process, but it is relatively expensive and has limited combinations of alloys that can be roll bonded successfully. Many high-strength alloys, such as the high Mg AA5000 series, are not easily bondable mainly because of their susceptibility to oxidation during the bonding process, which is carried out at elevated temperatures. Recently, a new technology referred to as ''Fusion Technology'' (Novelis–Solatens Technology Center, Spokane Valley, WA)[1,2] has been developed that produces clad material by direct chill (DC) casting. This process has few restrictions with regard to the combination of alloys that can be cast, and it allows clad sheet to be produced by essentially the same hot and cold rolling routes used for conventional, monolithic alloys. This means that in addition to brazing sheet and corrosion resistance sheet, packages can be fabricated that provide enhancement of other properties, such as improved surface properties and enhanced formability. Little information is found in the literature on the deformation of clad Al sheet, whereas many studies are available on sandwich panels and laminates that cover various aspects of deformation and fracture.[3–8] In many of these studies, the volume fractions of the individual components are equivalent, or close to equivalent, whereas in the clad packages of interest in the current work, the cladding volume fraction is 10 pct or less. This article examines the deformation of a clad package AA3003/AA6000, in which the high-ductility AlMn AA3000 alloy is clad onto and forms the surface of the higher strength automotive sheet AlCuMgSi AA6000.

DAVID J. LLOYD, Principal Scientist (retired), and MARK GALLERNEAULT, Senior Investigator, are with Novelis Global Technology Centre, Kingston, Ontario, Canada K7L 5L9. Contact e-mail: mark.gallereneault@novelis.com ROBERT B. WAGSTAFF, Director of Research, is with Novelis–Solatens, Spokane, WA 99206.
Manuscript submitted October 20, 2009.
Article published online May 26, 2010

II. EXPERIMENTAL DETAILS

Commercial clad sheet produced by the Fusion Technology consists of a core alloy laminated on its rolled surfaces by another clad alloy. Part of this study considers a DC ingot with a core alloy of AA6111 sandwiched between clad layers of AA3003 (each clad layer was 10 pct of the total package thickness). Sheet was fabricated via plant rolling to a 1-mm gauge after homogenizing to dissolve any coarse Mg_2Si and AlMgSiCu–Q phase formed during solidification, hot rolling to 5 mm, and then cold rolling. The final gauge sheet was solutionized to a T4 temper on a continuous annealing line (using a solutionizing temperature of 833 K (560 °C)) and then naturally aged for several weeks. Some sheet also was preaged for 8 hours at 353 K (80 °C) to produce the T4P temper, which is a more thermally stable material that does not extensively naturally age and provides an enhanced paint bake response. In addition, a one-sided clad sheet was examined—AA3003/X609 ingot that was laboratory fabricated to 1-mm sheet for this particular study. One-sided clad material has some advantages for certain experiments, as will be discussed in the text. In addition, the monolithic alloys also were processed to 1-mm sheet (using the same fabrication route as that used for the clad sheet) and tested for comparison. The chemical compositions of the alloys in the different packages are given in Table I. The yield strength of AA6111-T4P is about 150 MPa. whereas that of X609 is softer at

120 MPa (the T4 and T4P tensile properties are essentially equivalent). The tensile properties were examined using standard ASTM B557 2-cm gauge length tensile samples at a nominal strain rate of 10^{-3} s^{-1}, but the alloys are essentially strain rate insensitive for conventional testing of strain rates. In addition, the bendability of the sheet was investigated using mainly the wrap bend test; in this test, individual sheet samples were wrapped or bent around an ever-decreasing radius die until cracking was observable optically on the surface. The results then are expressed in terms of the minimum bend radius r (to which the sheet can be bent without exhibiting surface cracking) normalized by the sheet thickness t, yielding a value for r/t (*i.e.*, bendability improves with decreasing values of r/t). The wrap bend result is influenced by the sheet surface condition, and in the present experiments, the processed mill finish to the sheet was used. A second test also was used to obtain bending load–bend angle information, which can be obtained from the Cantilever bend test[9,10] (CBT). The bendability also varies with the bend axis orientation in the sheet; unless noted, the bendability was assessed in the transverse orientation, which means that the bend axis is parallel to the rolling direction. Bendability is usually lower in this orientation as opposed to bending transverse to the rolling direction.

III. THE INTERFACE

In most of the current commercial applications (which are predominantly for use in brazing processes), the interfacial strength, provided it maintains a reasonable level of integrity, is not critical because the sheet is not subjected to any severe forming operations. However, in the case of clad automotive sheet, forming can be extensive, and it is critical that the sheet does not delaminate. A detailed consideration of the interface is beyond the scope of the current article, but it is relevant to consider briefly the microstructure and estimate the strength of the interface. To do this, the single side clad AA3003/X609 is useful because slices can be cut from this ingot that are perpendicular to the casting direction, and if this slice is rolled, again, in a direction perpendicular to the casting direction, then the result is a compound sheet that consists of one part cladding and one part core. Tensile samples then can be cut to produce a compound tensile sample that includes the interface. Because of the different yield strengths of the core and cladding, the softer AA3003 cladding elongates somewhat more than the stronger X609 core, which results in some perturbation of the planar, as-cast interface, and the AA3003 section of the sheet is slightly thinner than the core alloy portion. However, the thickness profile along the sheet can be measured to allow for the thinning, and the interface remains essentially perpendicular to the applied tensile stress, so that by tensile testing and noting the failure position, some bounds on the interface strength can be obtained.

Figure 1 shows the microstructure of the as-cast interface; there is no sharp delineation of the interface, nor is there any evidence of porosity or oxide films. The solidification cells of the cladding alloy merge with those of the core without any apparent discontinuity. The figure also shows the interface region in the final, as-solutionized sheet, and again, the only indication of the interface is the microstructural change from the high density of coarse

Table I. Chemical Compositions of the Package Components in Weight Percent

Component	Si	Cu	Mg	Mn	Fe
AA6111	0.65	0.7	0.75	0.2	0.25
X609	1.2	0.5	0.4	0.2	0.2
AA3003	0.2	—	—	1.0	0.5

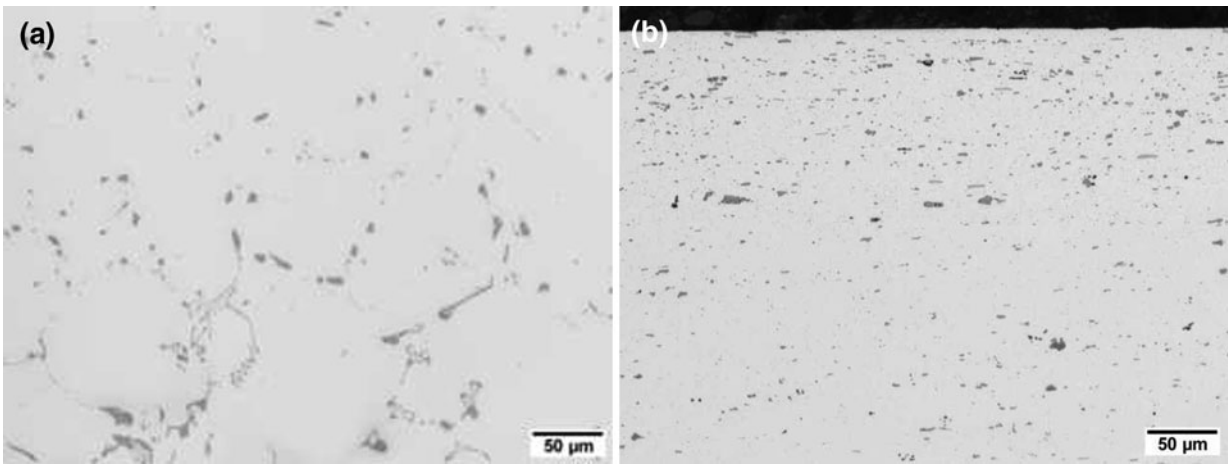

Fig. 1—Interface region of (*a*) as-cast AA3003/X609 and (*b*) fabricated to sheet and solution treated.

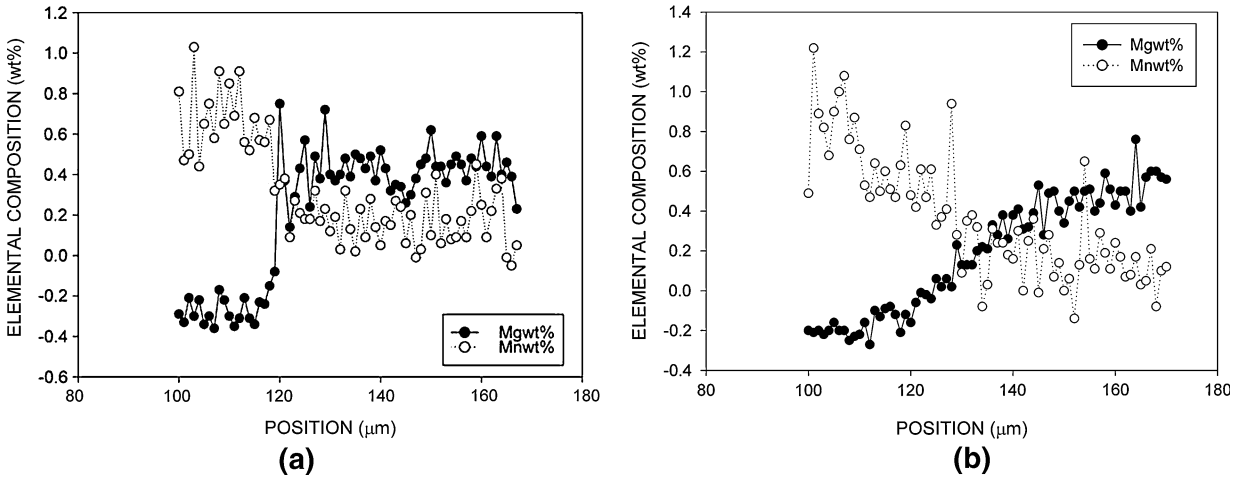

Fig. 2—Mg and Mn compositional profiles across the interface (*a*) and as-rolled (*b*) after solutionizing at 833 K (560 °C).

constituent particles in the AA3003 to the finer microstructure in the core alloy. Composition profiles were obtained from energy dispersive spectroscopic analysis (EDS) across the boundary in the final, as-rolled sheet and also, after solutionizing, are shown in Figure 2. For clarity, the analyses shown are just for the slowest diffusing species, Mn, and the fastest, Mg. It is apparent that the transition region from clad to core occurs across a distance of about 20 μms in the as-rolled sheet, and the profile is slightly broadened after solutionizing because of the diffusion occurring during the high-temperature solution treatment. It should be noted that the negative compositional values on the cladding side for Mg are a result of the normalization procedure and that some compositional peaks in Mn are a result of intermetallic particles in the analysis region. A more detailed analysis of the interface will be reported separately.

The compound sheet samples were tensile tested in the following conditions: as-rolled, T4 and artificially aged at 453 K (180 °C). The stress-strain curves for the monolithic AA3003 O-temper and X609–T4, as well as the T4 clad sample are shown in Figure 3, from which it can be observed that the yield and ultimate tensile strength (UTS) of the compound sample are close to those of the monolithic AA3003, which would be expected. Table II shows the yield and UTS values obtained for the other conditions. Since AA3003 is a nonheat-treatable alloy and comprises most of the compound sample, the compound sample tensile properties are largely unchanged by heat treatment. However, there is a significant increase in strength for the cold rolled condition because both components of the compound specimen increase their strength as a result of cold work. In this case, the compound sample achieves a maximum strength of 175 MPa. In all three conditions, the compound sample failed in the softer AA3003 component of the sample and away from the interface (Figure 4). From these data, it can be concluded that the interface has a strength of at least 175 MPa and that aging does not result in any embrittlement of the interface sufficient enough to result in premature interfacial failure.

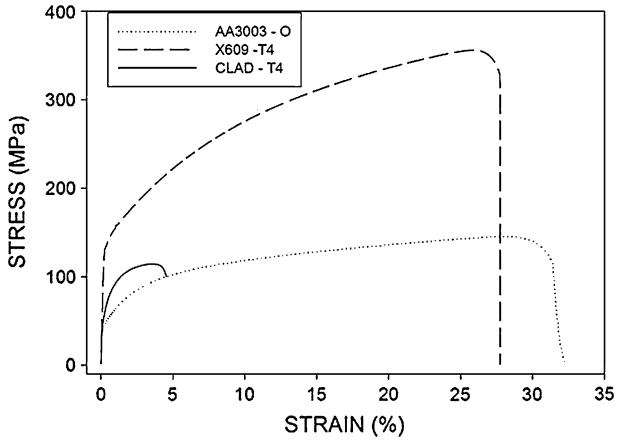

Fig. 3—Tensile stress-strain curves for compound T4 samples.

IV. TENSILE BEHAVIOR

The tensile stress-strain response of commercially processed, 50-μm (10 vol pct), double-sided clad AA3003/AA6111/AA3003 in the T4 temper is shown in Figure 5, along with those of the monolithic alloys of the package. The clad sheet has a slightly lower yield strength, which reflects the presence of the 10-vol pct AA3003 as well as a lower UTS but a somewhat increased tensile elongation. Clad sheet is a laminate, and because there is a high interfacial strength, the clad sheet should deform under equistrain conditions, and the rule of mixtures (ROM) should apply in terms of the yield strength as follows:

$$\sigma_Y = \sigma_{CL} f_{CL} + \sigma_{CR}(1 - f_{CL}) \quad [1]$$

where σ_Y, σ_{CL}, and σ_{CR} are the yield strengths of the clad sheet, the monolithic cladding, and the monolithic core alloys, respectively, and f_{CL} is the volume fraction of the cladding alloy. To assess the appropriateness of Eq. [1], an ingot of AA3003/X609 was scalped to various extents prior to rolling to 1-mm sheet, so that several volume fractions of cladding were obtained. Figure 6 shows the variation in yield strength with the

Table II. Tensile Strengths of Compound AA3003/X609 Samples

Specimen	Condition	Yield Strength (MPa)	UTS (MPa)
AA3003	O - Temper	47	112
X609	T4	137	277
Compound	As-Rolled	165	175
Compound	T4	64	110
Compound	Aged 2 h/453 K (180 °C)	64	111
Compound	Aged 8 h/453 K (180 °C)	72	113

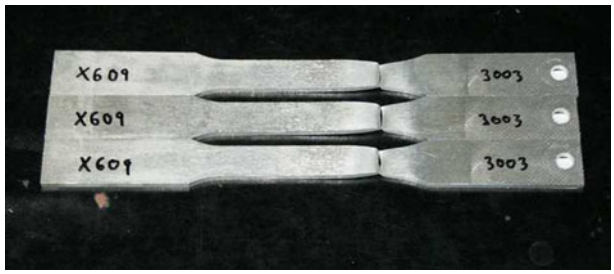

Fig. 4—Failed compound tensile samples.

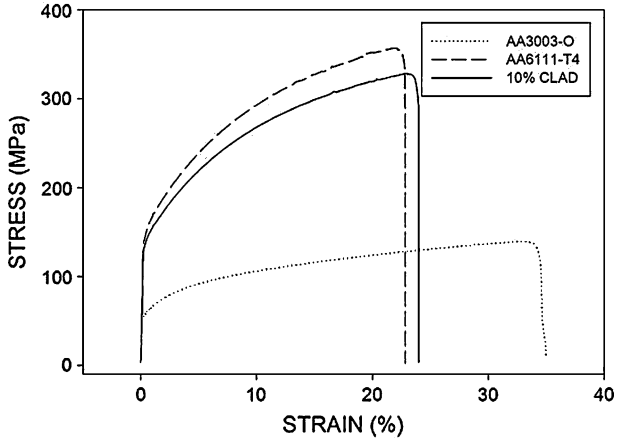

Fig. 5—The stress-strain curves for AA3003/AA6111/AA3003 and the monolithic components of the clad package.

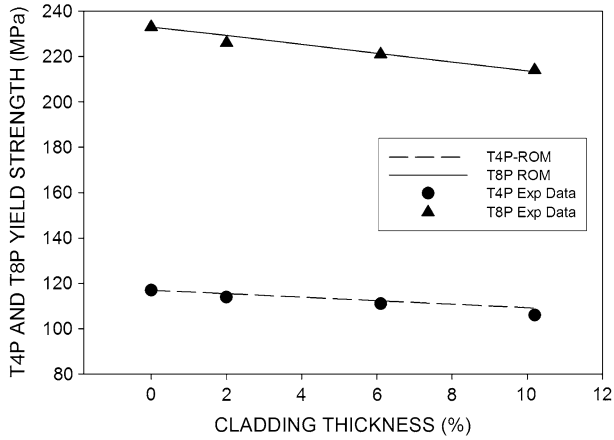

Fig. 6—ROM representation of the yield strength of the clad sheet.

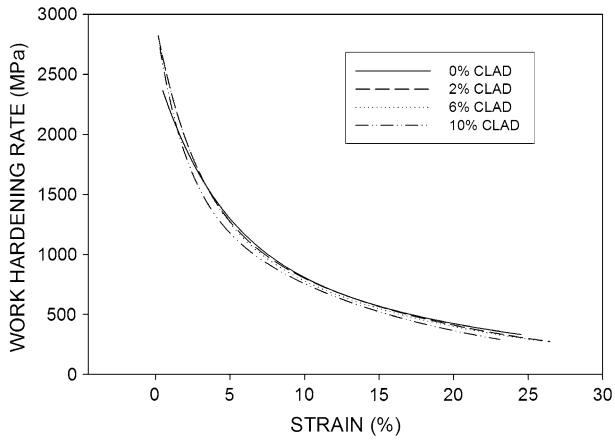

Fig. 7—Work hardening response for different levels of cladding.

volume fraction of cladding, and the agreement with the ROM is good. This figure also shows data for sheet in the paint bake temper, which is the condition the sheet would have in the final product (the paint bake condition was simulated by stretching the clad sheet 2 pct followed by 30 minutes at 450 K (177 °C)). The ROM also describes this data well.

The stress-strain response of Al alloys often is represented by the power law ($\sigma = K\varepsilon^n$), even though it is not an accurate representation of the deformation. In the current clad sheet, the value of n is 0.3, which is comparable with the monolithic X609 sheet. If the actual work hardening rate with strain is considered for different cladding levels, then there is little difference between the different packages, as shown in Figure 7. So at these levels of cladding, the work hardening rate in tension is affected only slightly by the cladding. Another point of interest is the artificial aging response of the clad sheet, and Figure 8 shows the 453 K (180 °C) aging curve for AA3003/X609 with a 60-μm cladding. The aging kinetics are essentially equivalent; the clad sheet exhibits the slightly lower yield strength as a result of the cladding of AA3003, which does not respond to aging. The decline in tensile elongation with aging was also the same in the two materials; in the clad sheet, the uniform elongation decreases from 29 pct in the solutionized condition to 11 pct in the peak aged condition.

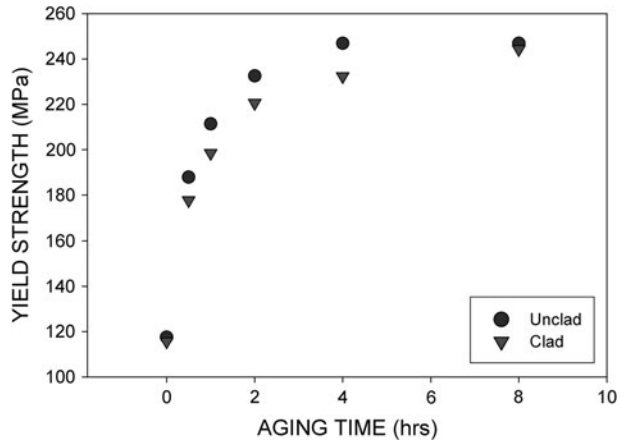

Fig. 8—The 453 K (180 °C) aging curve for monolithic and 60-μm clad sheet.

V. BENDING BEHAVIOR

Bending is an important deformation mode in many applications, and Al automotive sheet tends to have inferior bendability compared with automotive steel sheet. Several recent publications[11,12] have considered various aspects of bending in Al alloys, and because bendability is controlled by surface cracking, a ductile clad layer at the surface has the potential to improve bendability for this application. Figure 9 shows the CBT bending load trace for monolithic AA6111 and AA3003/AA6111/AA3003–T4P clad sheet bent in the transverse direction (*i.e.*, the bend axis is in the rolling direction). The bending load is higher in the monolithic sheet and decreases after a bend angle of 75 deg, which corresponds to the angle at which cracks begin to form on the specimen surface. The clad sheet shows no sharp bending load decline up to a bend angle of 120 deg, which is the maximum angle that can be achieved in the CBT. There is no evidence of surface cracking up to this angle in the clad sheet, which supports the view that a ductile cladding can improve bendability. Because, in practice the sheet is formed prior to bending, it is of interest to investigate the bendability of sheet that has been prestrained prior to bending. Figure 10 shows the wrap bend results for AA3003/AA6111/AA3003, and it confirms the CBT results; the clad sheet displays about 50 pct improvement in bendability across the complete prestrain range. This package has 10-vol pct cladding, and it is of interest to investigate the influence that the extent of cladding has on bendability. To do this, the AA3003/X609 package was used. Because this material is clad on one side, the comparison between monolithic and clad sheet can be assessed simply by either testing with the "cladding side up" in the bend test to give the bendability of the clad sheet or with the "core side up" to obtain the bendability of the core alloy. Figure 11 shows the variation of bendability with cladding level. Again, the cladding improves bendability, in this case, by about 30 pct for 2-vol pct cladding and by 50 pct for the 6- and 10-vol pct cladding levels, respectively, which is comparable with the effect observed in the double-sided AA3003/AA6111 package. Once the material has been prestrained, the 6- and 10-vol pct cladding levels give the same bendability. The influence of cladding level on the bendability for the two prestrains of 0 pct and 10 pct is shown specifically in Figure 12, where it is clear that there is a gradual improvement in bendability

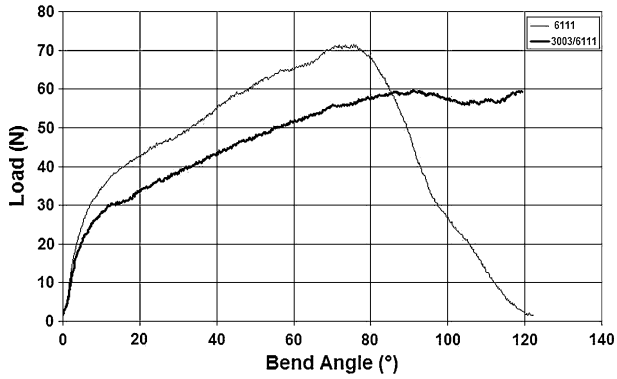

Fig. 9—CBT traces for monolithic AA6111-T4P and AA3003/AA6111/AA3003-T4P.

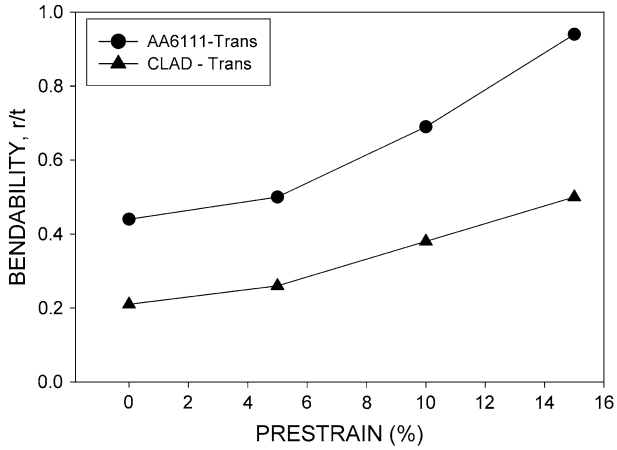

Fig. 10—Bendability r/t of AA3003/AA6111/AA3003-T4, with 10-pct cladding and monolithic AA6111-T4P.

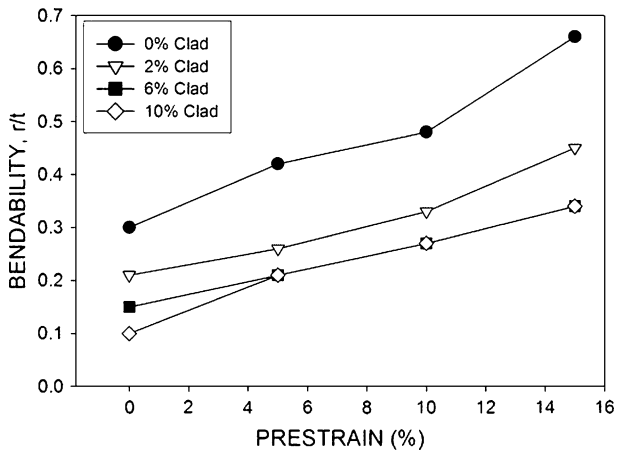

Fig. 11—Influence of cladding volume fraction on bendability.

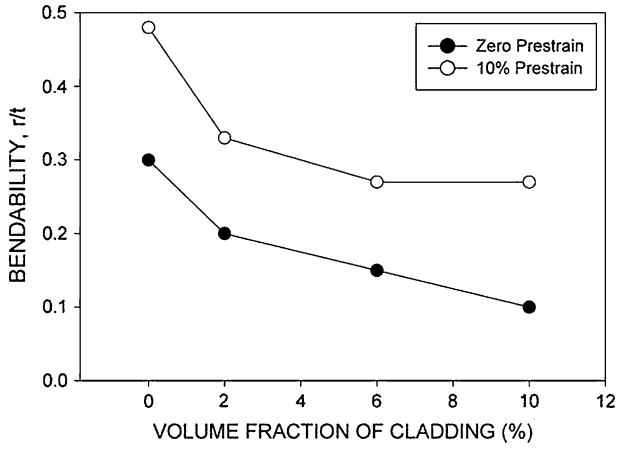

Fig. 12—Influence of cladding level on bendability.

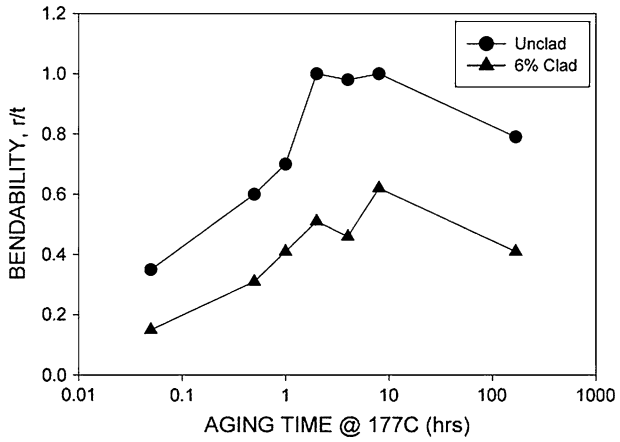

Fig. 13—The influence of cladding with aging at 450 K (177 °C) for AA3003/X609, with 6 pct cladding.

with an increasing cladding level up to about 10 pct for all extents of prestrain.

Finally in regard to bending, it is of interest to see whether the improvement in bendability with cladding is maintained in aged material, which is shown for AA3003/X609, with 6 vol pct cladding in Figure 13. Clearly, the improved bendability in clad sheet is maintained throughout the complete aging period, even though the bendability of the clad sheet does decrease with increased aging time until overaging occurs.

VI. DISCUSSION

The interface study demonstrates that the Fusion Technology produces a clean, high-strength interface that has no sharp delineation between the cladding and the core. This is not surprising because the process is a molten metal one, in which the liquid cladding alloy is brought into contact with the solid core alloy removing any surface skins and detritus and locally remelting the surface region of the core ingot prior to solidifying. This results in a local transition from the composition of the

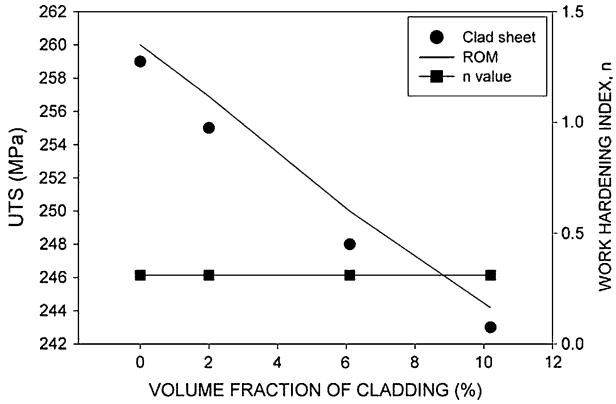

Fig. 14—ROM compared with the experimental results for the UTS of AA3003/X609 clad sheet and the corresponding *n* value.

cladding alloy to that of the core, and the sharp interface is not present typically observed in roll-bonded sheet. The failure of the compound tensile samples in the softer AA3003 component is expected because plasticity predominantly should occur in the softer alloy, and failure occurs when the UTS of AA3003 is reached. The maximum UTS of 175 MPa in cold rolled AA3003 is a lower bound for the strength of the interface region in this package, which is very high for a clad system. However, it should be noted that the authors could not find any reliable interfacial strength results for roll-bonded sheet in the literature.

The deformation mechanics of laminates have been established for some time,[13] but the laminates considered usually have much higher volume fractions of the second component than the 10 vol pct of the present sheet. Nevertheless, if the two components are well bonded, then the assumption of equal strains is appropriate and the elastic modulus and yield strength obey the ROM (Eq. [1]). The present clad sheet is consistent with this hypothesis, as shown in Figure 6. The situation in regard to work hardening, and hence to UTS, is more complex; in addition to the stress-strain behavior expected for the appropriate volume fraction of the monolithic components, stresses are generated from the plastic strain distribution between the two components, and the constraints developed because of the different plastic response of the clad and core components. This will result in deviations from the ROM behavior. The constraint component can become particularly important at higher levels of plastic strain. As shown in Figure 14, the simple ROM description overestimates the UTS of the clad sheet. The previous results for work hardening rate (Figure 7) show that the work hardening rate decreases with an increasing cladding level, even though the decrease is not large. Both results indicate that a larger proportion of the strain is being accommodated in the softer, lower work hardening rate AA3003. Also shown in the figure is the corresponding variation in the work hardening index *n*, and this does not change with the level of cladding, but as noted previously, the power law representation of the stress-strain behavior is an approximation. In principle, the

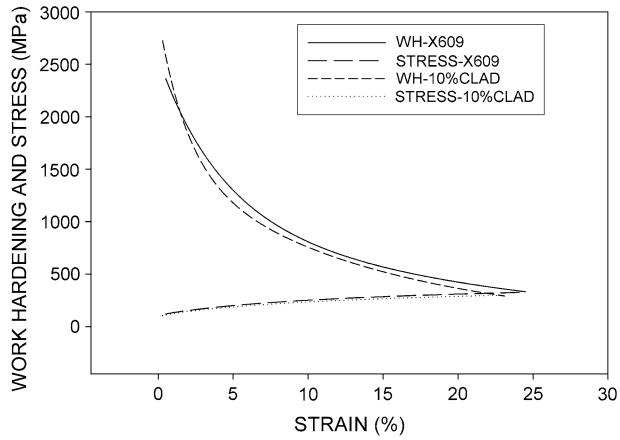

Fig. 15—Considère plots for monolithic X609 and 10-pct clad sheet.

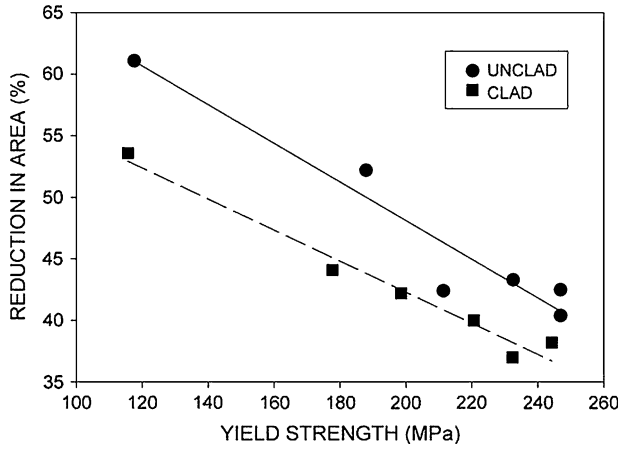

Fig. 16—Variation in the fracture strain with yield strength for aged X609 and 6-pct clad AA3003/X609.

relative strength and work hardening behavior of the two components significantly can affect the tensile response of the clad sheet, can influence the distribution of strain in the different components, and can control the instability/necking strain as well as the fracture strain. In the AA3003/AA6111/AA3003 package shown in Figure 5, the uniform elongation of the clad sheet is slightly larger than that of the monolithic AA6111, but this will depend on the combination of alloys in the package. The upper limit for the instability strain is given by the following Considère criterion:

$$\sigma = {}^{d\sigma}/_{d\varepsilon} \qquad [2]$$

where σ is the flow stress at strain ε, and $d\sigma/d\varepsilon$ is the work hardening rate. Figure 15 shows the Considère plots for X609 and the 10-vol pct clad sheet, and the intersection of the $d\sigma/d\varepsilon$-ε plot with the σ-ε plot indicates the strain at which necking initiates. In this case, the plots indicate that the clad sheet should have a slightly lower uniform tensile strain; the experimental results for the transverse orientation gave a uniform strain, $\varepsilon_U = 29$ pct for X609 and $\varepsilon_U = 27$ pct for 10-vol pct clad sheet. This result is consistent with Figure 15, considering that the figure indicates the necking initiation strain, but a variation of 2 pct is within the typical scatter of such data. However, the necking behavior is expected to be dependent on the relative rates of work hardening of the cladding and core alloys as well as the volume fraction of the cladding. If the cladding alloy has a significantly higher work hardening rate than the core alloy, then the uniform strain should be enhanced, and this theory is supported by recent finite element modeling.[14]

In addition to the tensile elongation, there are situations in which the fracture strain or the reduction in area at fracture (RA) may be important. Recent work has suggested that RA scales with the yield stress for Al alloys,[15] and it is of interest to see whether this is also the case with clad sheet. The yield stress range is too small to consider T4 results, and these are of varying cladding levels, but artificially aged AA3003/X609 gives an extensive yield stress range for consideration. The results from this package are shown in Figure 16. The clad sheet does scale with the yield stress, which is consistent with monolithic alloys, and the fracture strain is lower in the clad sheet, so the detailed fracture mechanism is modified in the presence of a cladding, which is important when the bending behavior is considered.

Bending in monolithic Al alloys is still not well understood, but recent publications[10–12] have shown that the surface develops severe topographical features both in the matrix, where strain localization in severe bands develops, and at grain boundaries. In addition, cracking is initiated in these regions. The surface strains that develop can be large in comparison with those encountered in tensile deformation. Because a bend surface is a "free, unconstrained" surface, with a strain gradient that decreases from the surface through the thickness of the sample to the neutral axis, the situation is different from the localized necking situation in tensile deformation. Microstructural mechanisms, such as intermetallic particle fracture and voiding, occur as they do in other failure modes.

The surface strain at a particular r/t in bending is expressed as follows:

$$\varepsilon_s = \ln\left[(r+t)/\left(r+{}^{t}/_{2}\right)\right] \qquad [3]$$

where r is the bend radius and t is the sheet thickness These are lower bound strain values for a static neutral axis, but if the axis moves toward the compression side during bending, which is likely, the bending strain is expressed as follows:

$$\varepsilon_{SN} = \ln[(r+t)/(r+g)] \qquad [4]$$

where

$$(r+g) = [r(r+t)]^{1/2}$$

Equations [3] and [4] can be used to estimate the strain at any position in the sheet, including the maximum strain in the core at the clad-core transition. This can be done by substituting $t = (t_o - t_{cl})$, where t_o is the

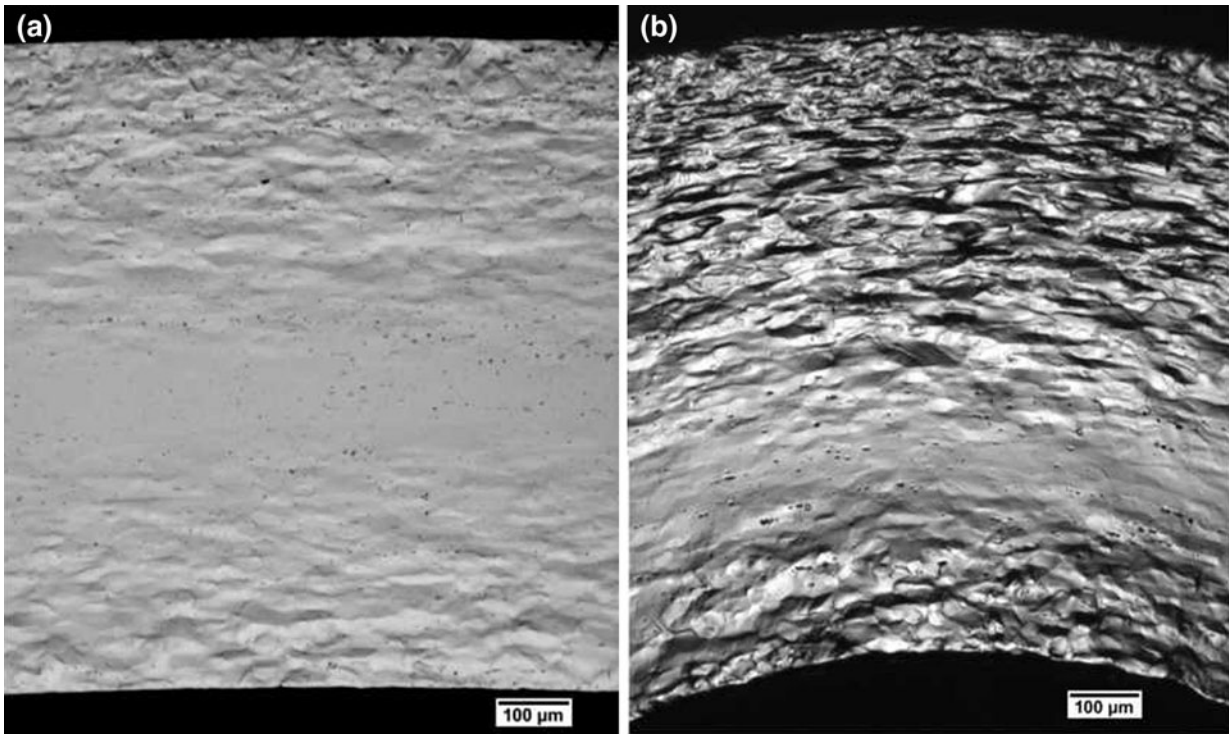

Fig. 17—The edge topography development with bending angle (*a*) 18 deg and (*b*) 100 deg.

thickness of the sheet and t_{cl} is the thickness of the cladding. Before doing this, it is necessary to establish whether Eq. [3] or Eq. [4] is appropriate, and to do this, the edge of the bend sample was polished prior to bending through a range of angles and observing the change in topography in the through thickness section. Figure 17 compares the topography at bend angles of 18 deg and 100 deg. The neutral axis is indicated clearly by the region of low roughness close to the center of the sheet for 18 deg, and this region moves toward the inner radius of the sheet for the 100 deg bend. So in this case, the neutral plane moves downward through the sheet with bending and Eq. [4] is appropriate. Figure 18 shows the variation in the maximum strain achieved in the core at the interface for the r/t results at the different levels of cladding shown previously in Figure 11 for zero prestrain. AA3003–O temper has $r/t = 0$, so it can be bent back completely on itself without bend failure. The tensile RA is 78 pct to 80 pct, which is equivalent to a true fracture strain ε_F of about 1.6, so bend failure occurs at a much lower r/t and a lower surface strain than in monolithic AA3003. X609 has an $r/t = 0.3$ and a tensile RA $\cong$ 61 pct, $\varepsilon_F \cong 0.9$ in the T4 temper. The unclad X609 is failing in bending at a calculated surface strain of 0.73—somewhat below the tensile fracture strain—but this failure strain is increased to 1.2 for a 10-vol pct cladding level, which is 47 pct greater than the strain in unclad sheet and is 30 pct greater than the tensile fracture strain of X609. However, all these strain levels are less than the tensile fracture strain of monolithic AA3003-0.

For monolithic material, Datsko and Yang[16] suggested that failure in the outer fiber of a bend sample occurs when the strain in the outer fiber reaches the fracture strain of the material in tension and derived the following expression:

$$r/t = \left(\frac{C}{RA} - 1\right) \quad [5]$$

where RA is the tensile reduction in area (in pct) at fracture and C is a constant. For materials in which the neutral axis remains at the center of the sheet, such as materials with limited ductility, they derived C = 50, whereas for a moving neutral axis, they suggested C = 60. Previous results[10,12] on bending in Al alloys have shown general agreement with Eq. [5], but

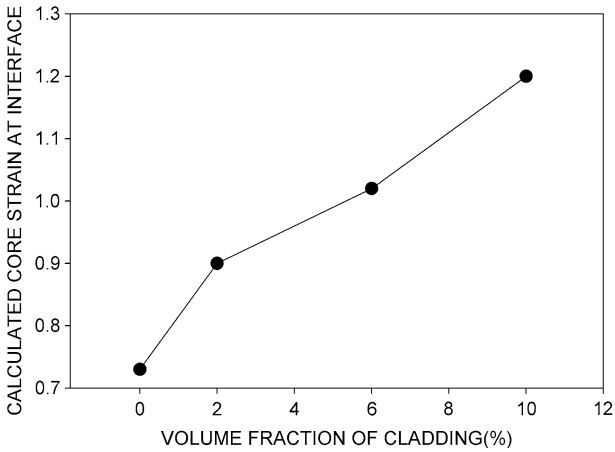

Fig. 18—Calculated strain in the core close to the interface for different volume fractions of cladding and zero prestrain.

with a C value of about 70. Equation [5] is an approximation for the following derived theoretical equation:

$$r/t = \frac{(100 - RA)^2}{200RA - RA^2} \quad [6]$$

As a result, the constant C provides for the numerical approximation of the theoretical expression. In addition, bending is a deformation in plane strain, as is the theoretical analysis, but the RA measurements, as in the present article, usually are made after tensile deformation. The fracture strain is strain-path dependent, with the tensile fracture strain generally being greater than the fracture strain in plane strain, and the difference varying with alloy as a result of the role of microstructure on the details of the fracture process. C also accounts for this approximation and can vary to some extent from alloy to alloy.

By considering the bendability of the monolithic and 6 vol pct clad sheet using the fracture strain results shown previously in Figure 16, a comparison with Eq. [5] can be made, as shown in Figure 19. The monolithic X609 has a value of C ≅ 75, whereas the 6-vol pct clad sheet has C ≅ 65. Also shown in this figure are the T4 results for the three levels of cladding, which cluster around the theoretical curve. Considering that the measurements are made on sheet samples in which the reduction in area is not measured as accurately as in the usual cylindrical sample, the agreement with Eq. [5] is good, and the bendability clearly scales with the fracture strain. This figure also demonstrates the higher fracture strain required in X609 to achieve equivalent bendability to that of the clad sheet.

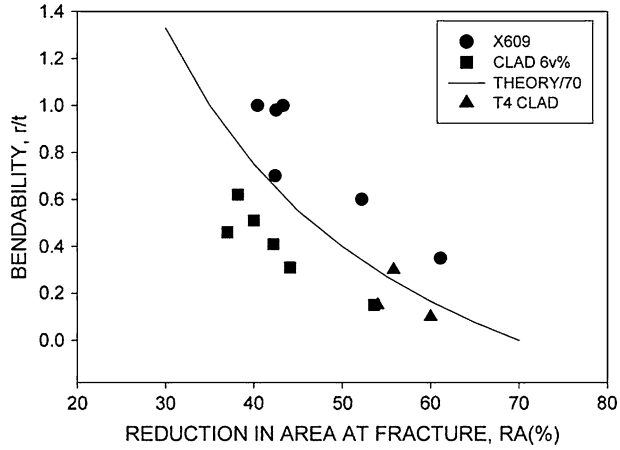

Fig. 19—Variation in bendability with aged tensile fracture strain and T4 sheet.

These results demonstrate that the fracture behavior in bending is drastically modified by the presence of a ductile clad layer. The strains achieved in the core in bending are significantly larger than the fracture strain of monolithic sheet, so the 6000 core alloy should be extensively damaged in regions of maximum bending strain prior to the observed bending failure at the surface. Figure 20(a) shows a sample of AA3003/X609 that has just reached bend failure; the crack has propagated through the AA3003 cladding, and there is no indication of failure in the clad–core transition. Figure 20(b) is away from the surface cracked region and shows extensive damage in the form of particle cracking and particle/matrix voiding, so the core has developed extensive damage, as expected, from the calculated bending strains and the tensile fracture strains.

The introduction of a ductile phase to improve the fracture resistance of a relatively brittle material has been studied extensively, particularly in laminates and ceramic composites,[17,18] but these are rather different situations than the present case. However, Lewandowski *et al.*[19,20] have reported an improvement in bendability and toughness by cladding a particle-reinforced Al metal matrix composite with a soft AA1100 Al alloy, consistent with the present results. One common theme in all work on increasing fracture resistance by introducing a ductile phase is the ability of the ductile component to blunt the crack propagating in the more brittle component.

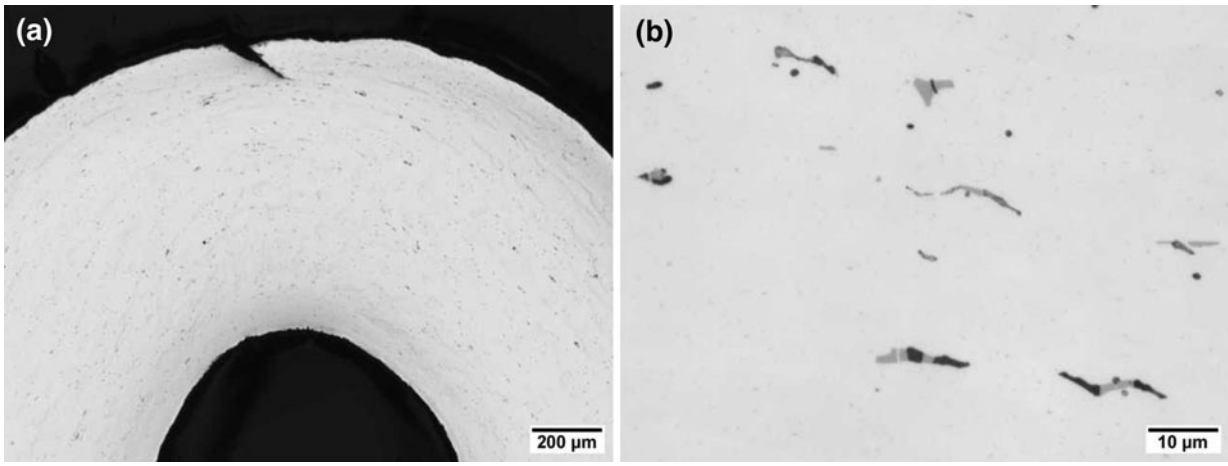

Fig. 20—Bend failure (*a*) and surface crack (*b*) damage associated with intermetallic particles in the core region away from the crack, AA3003/X609-T4.

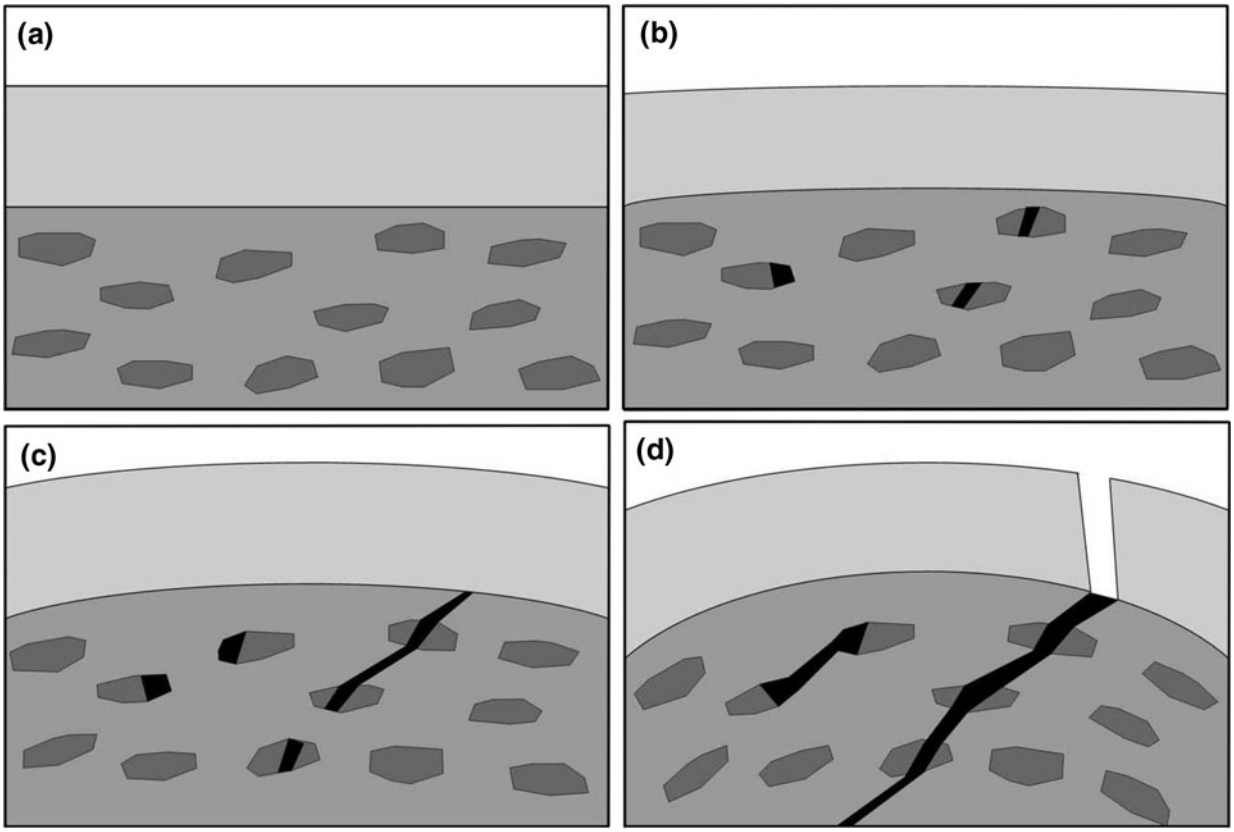

Fig. 21—Schematic of bend fracture path progression, (*a*) through (*d*), in clad sheet.

Although the core alloy component is not "brittle" in the sense of materials considered in most of these studies, AA6111 and X609 have significantly lower fracture strains than the AA3003, and because the cladding–core transition region is of high strength, the ductile cladding is effective in blunting cracks nucleated in the core and propagating to the highly strained bend surface. The bend failure mechanism is shown diagrammatically in Figure 21. As bending progresses, intermetallic particle cracking and voiding occurs in the AA6xxx core in the highly strained regions close to the core–clad transition region. Eventually the bend angle generates sufficient stress and strains for a crack to nucleate and propagate in the core toward the surface of the bend sample where it effectively is blunted by the ductile cladding. As bending continues, additional damage and crack propagation toward the inner radius of the sheet occurs in the core, whereas the plasticity localizes in the cladding in the region of the core crack below the cladding. Eventually, the cladding fails and the crack propagates, mainly by shear in the present case, though the cladding can experience bend failure. Deformation in bending is particularly susceptible to shear localization.[21] Essentially no damage is developed in the AA3003 cladding prior to final fracture, but areas of local thinning, which appear as surface rumpling, are formed, as is shown in Figure 20(a).

The cladding thickness will influence the bend angle at which cladding failure occurs in the following ways: first, as the cladding thickness increases, the effective radius for the core decreases, requiring a higher strain and, hence, bend angle to produce failure, and second, the thicker the cladding, the higher the stress concentration associated with the core crack will have to be to produce cladding failure. As a result, the required bend angle increases with cladding thickness, as shown by the present results. Obviously a cladding thickness finally will be reached where bending is controlled by the bending behavior of the cladding itself, but this would be accompanied by a much lower strength sheet. The effect of prestraining is important but also complex; prestraining strain hardens both the cladding and the core; however, because the work hardening rates for the two alloys are different, the change in the relative flow stresses also will be different. In addition, prestraining can generate damage, such as cracked particles and voiding in both the cladding and the core prior to bending. In monolithic alloys, the bendability deteriorates with prestrain. The failure model suggested requires that the more ductile, lower strength cladding blunts any cracking in the core and inhibits its propagation to the surface. Prestraining will increase the propensity for cracking in the core during bending, and it also will reduce the efficacy of the cladding to blunt any propagating cracks because the prestraining increases the cladding flow stress and reduces its ductility. The results indicate that the bendability after prestraining is essentially the same at 6 and 10 vol pct cladding levels, which suggests that the degree of blunting is the same after prestraining at the two levels

and that the efficacy of blunting has saturated. This is physically reasonable, but further experiments are required to explore this in more detail.

An interesting aspect of this bend failure mechanism is that it is dependent on the bend crack development in the core being one of stable, slow crack growth that can be blunted by the ductile cladding. Some Al alloys fail in bending by unstable, fast fracture, which occurs in some of the higher strength AA2000 and AA7000 series alloys. In these systems, the crack energy release rate in the core can be high, and a ductile cladding may be less capable of providing effective blunting without being thick. Some recent results by the authors on AA1200/AA2024 support this view.

VII. SUMMARY

The current investigation shows that producing clad Al sheet using the DC casting Fusion Technology route results in clad sheet with a high interfacial strength of at least 175 MPa in the current AA3000/AA6000 package. The tensile properties of the sheet obey the ROM for composite materials, and the bendability of the sheet is improved significantly. Failure of the sheet is initiated in the lower ductility core, where damage in the form of cracked intermetallic particles and particle/matrix voiding occurs, with the resulting crack in the core eventually nucleating failure in the cladding. The bendability improves with an increasing volume fraction of cladding, but this improvement is accompanied by a decrease in the sheet strength, so a cladding total thickness equivalent to 10 vol pct seems to be a good compromise for a combination of strength and bendability.

ACKNOWLEDGMENTS

The authors are grateful to Novelis for permission to publish this work and to their colleagues in the Novelis Global Technology Centre, Kingston, Ontario, Canada and Solatens, Spokane, WA, who provided technical support for various parts of this study.

REFERENCES

1. R.B. Wagstaff, D.J. Lloyd, and T.F. Bischoff: *Mater. Sci. Forum*, 2006, vols. 519–521, pp. 1809–14.
2. M.D. Anderson, K.T. Kubo, T.F. Bischoff, W.J. Fenton, E.W. Reeves, B. Spendlove, and R.B. Wagstaff: Patent US 7,472,740.
3. A.P. Kofman, P.O. Pashkov, and A.A. Yavor: *Metalloveenie i Termicheskaya Obrabotka Metallov*, 1966, no. 10, pp. 16–18.
4. A.G. Atkins and A.S. Weinstein: *Int. J. Mech. Sci.*, 1970, vol. 12, pp. 641–57.
5. E.A. Almond, J.D. Embury, and E.S. Wright: *ASTM STP452*, 1968, pp. 107–29.
6. R. Hawkins and J.C. Wright: *J. Inst. Metals*, 1971, vol. 99, pp. 357–71.
7. C.K. Syn, D.R. Lesuer, J. Wolfenstine, and O.D. Sherby: *Metall. Trans. A*, 1993, vol. 24A, pp. 1647–53.
8. T. Mori and S. Kurimoto: *J. Manuf. Sci. Eng.*, 1998, vol. 120, pp. 179–84.
9. A. Selcuk and R.D. Rawlings: *J. Test. Evaluat.*, 1991, vol. 19, pp. 349–58.
10. D.J. Lloyd, D. Evans, C. Pelow, P. Nolan, and M. Jain: *Mater. Sci. Technol.*, 2002, vol. 18, pp. 621–27.
11. J. Sarkar, T.R.G. Kutty, D.S. Wilkinson, J.D. Embury, and D.J. Lloyd: *Mater. Sci. Eng. A*, 2004, vol. A369, pp. 258–66.
12. D.J. Lloyd: *Proc. James T. Staley Symp. Al Alloys*, ASM, Indianapolis, IN, 2001, pp. 161–65.
13. J.C. Halpin: *Primer on Composite Materials: Analysis*, Tecnomic Publishing Co. Inc., Lancaster, PA, 1984, pp. 35–67.
14. X.X. Chen, P.D. Wu, D.J. Lloyd, J.D. Embury, and Y. Huang: McMaster University, Hamilton, Ontario, unpublished research, 2009.
15. D.J. Lloyd: *Scripta Mater.*, 2003, vol. 48, pp. 341–44.
16. J. Datsko and C.T. Yang: *J. Eng. Ind. Trans. ASME*, 1960, pp. 309–14.
17. J.D. Kuntz, G.-D. Zhan, and A.K. Mukherjee: *MRS Bull.*, 2004, pp. 22–27.
18. J. Kajuch, J. Short, and J.J. Lewandowski: *Acta Metall. Mater.*, 1995, vol. 43, pp. 1955–95.
19. L. Yost Ellis and J.J. Lewandowski: *J. Mater. Sci. Let.*, 1991, vol. 10, pp. 461–63.
20. L. Yost Ellis and J.J. Lewandowski: *Mater. Sci., Eng. A*, 1994, vol. A183, pp. 59–67.
21. R. Becker: *J. Appl. Mech.*, 1992, vol. 59, pp. 491–96.